

Salt mechanics

Authors: Dr. Jörn Wichert, Prof. Dr. habil. Heinz Konietzky, Dr. Christian Jakob
(TU Bergakademie Freiberg, Geotechnical Institute)

1	Genesis of salt deposits	2
2	Utilization of salt rocks.....	5
3	General behaviour.....	5
4	Elastic behaviour	8
5	Visco-plastic behaviour.....	10
6	Constitutive models for salt rocks.....	17
1.1	Basic Models	19
1.2	Basic rheological models.....	21
1.3	Advanced and complex models.....	23
7	References	29

1 Genesis of salt deposits

Salts are evaporitic rocks, comprising variations of calcite, gypsum, anhydrite, halite, sylvite, carnallite, polyhalite, kainite and kieserite. Among all, halite (NaCl) is the most common salt with about 90 %.

Sedimentation

Salinification takes place in flat marine environment with water depth of up to several hundreds of meters due to evaporation. Seawater is a brine solution with about 3.45 % by mass of solved salt, which contains four main cations Na^+ , K^+ , Mg^{2+} and Ca^{2+} and four main anions Cl^- , SO_4^{2-} , Br^- and HCO_3^- (Table 1).

Solved salt minerals can precipitate and form salt deposits. App. 90 % of the salt deposits worldwide are halite (NaCl). Rock salt consists mainly of halite with some impurities like polyhalite, kieserite, anhydrite or clay. It is a poly-crystalline rock. It is a pre-requisite for the development of a salt deposit, that evaporation exceeds precipitation and inflow by rivers or groundwater. 100 m vaporized seawater creates about 1.5 m salt deposit. Figure 1 illustrates the genesis of seawater based salt deposits as it is typical for Zechstein.

Table 1 Mass percentage of solved main salt ions in seawater (Wright & Colling, 1995).

Solved ions	Mass ratio to water / %
Chloride, Cl^-	55.04
Sulfate, SO_4^{2-}	7.68
Hydrogen Carbonate, HCO_3^-	0.41
Bromide, Br^-	0.19
Sodium, Na^+	30.61
Magnesium, Mg^{2+}	3.69
Calcium, Ca^{2+}	1.16
Potassium, K^+	1.10

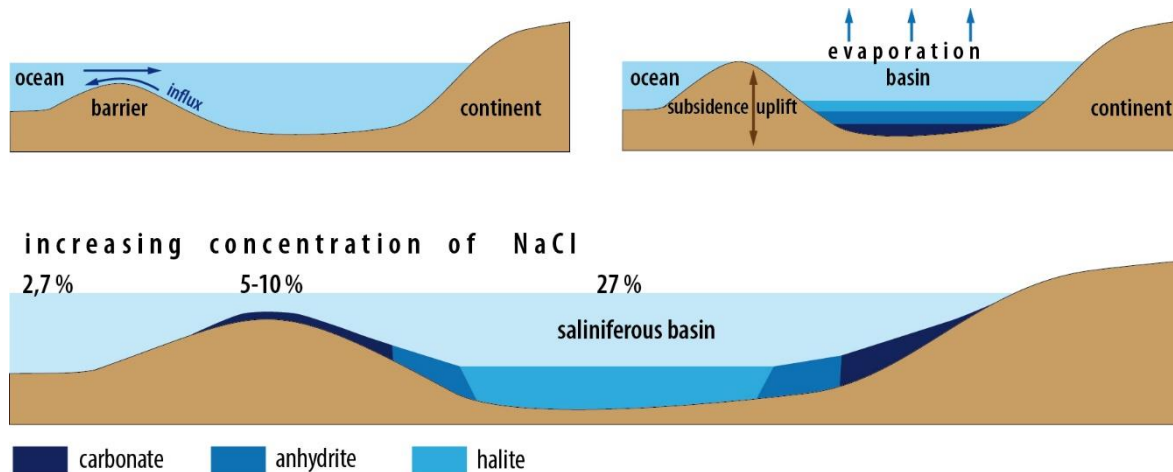


Figure 1: Scheme to illustrate genesis of salt deposits und salinity in dependence on the position inside the sedimentation space.

It is remarkable that the dissolved salts in the sea do not correspond to the vaporized salt deposit. The easier solvable salts (potash and magnesium salt and partly also halite) are under-represented. This is caused by the genesis illustrated in Figure 1. A typical sedimentation sequence is:

- Clay
- KCl
- NaCl; CaCl₂; MgCl₂
- CaSO₄ und MgSO₄ (sulphatic rocks)
- Carbonates (CaCO₃) (carbonatic rocks)
- Clay, salty clay

Halokinesis and Tectonic

Halokinesis is a process connected with gravity driven salt movements, which leads often to a diapir like salt uplift which ends in a salt dome structure. Such a process can get started because salt rocks can flow (creep) even under low differential stresses.

Pre-requisites for halokinesis are a minimum thickness of the salt rock layer of about 300 m, an inclination of the salt rock layer basis of more than 1° and a thickness of the overburden of more than 1000 m to create the necessary pressure. In addition, a significant density contrast between salt rock layer and overlying rock formations is necessary. Also, the temperature plays a significant role, because viscosity of salt decreases with increasing temperature.

Tectonic deformation of salt rocks are connected to compressional and/or extensional deformation regimes that means primarily horizontal forces. It happens, that sedimentation and tectonic deformation occur in sequence, which leads to complex depositional features.

Both processes, halokinesis and tectonic deformations, lead to the so-called diapirism. These diapirs can have different shapes according to different tectonic regimes (Figure 2). One can distinguish between reactivated and active diapirism. During reactivated diapirism extension leads to graben structures (fig. 3). If a reactivated diapir has

reached a certain uplift it will influence the tectonic regime in an active manner. This is called active diapirism. Diapirism can also be observed under compressional tectonic regimes characterized by dominating horizontal forces (Figure 4). Diapirs and salt rocks in general suffer often subsrosion (underground solution processes), which leads to subsrosion planes at the upper parts of the diapir.

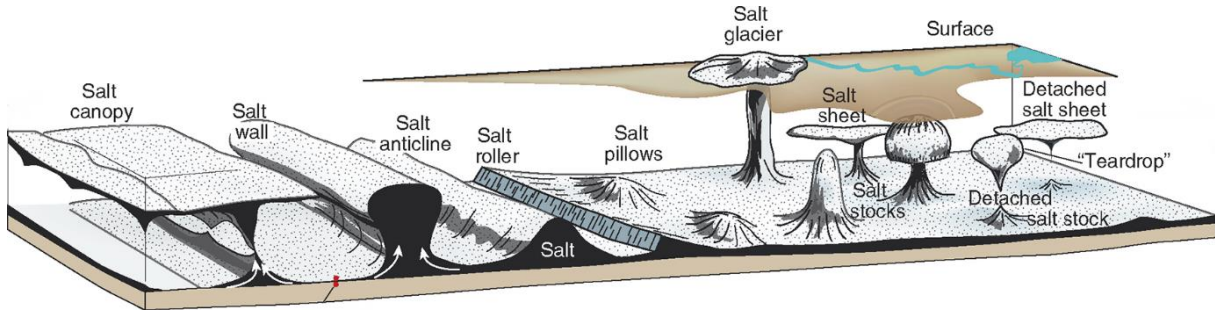


Figure 2: Typical diapir shapes (Fossen, 2016).

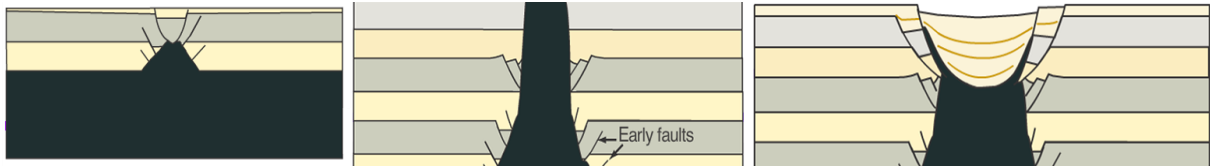


Figure 3 Uplift and drop of a diapir in an extensional regime.

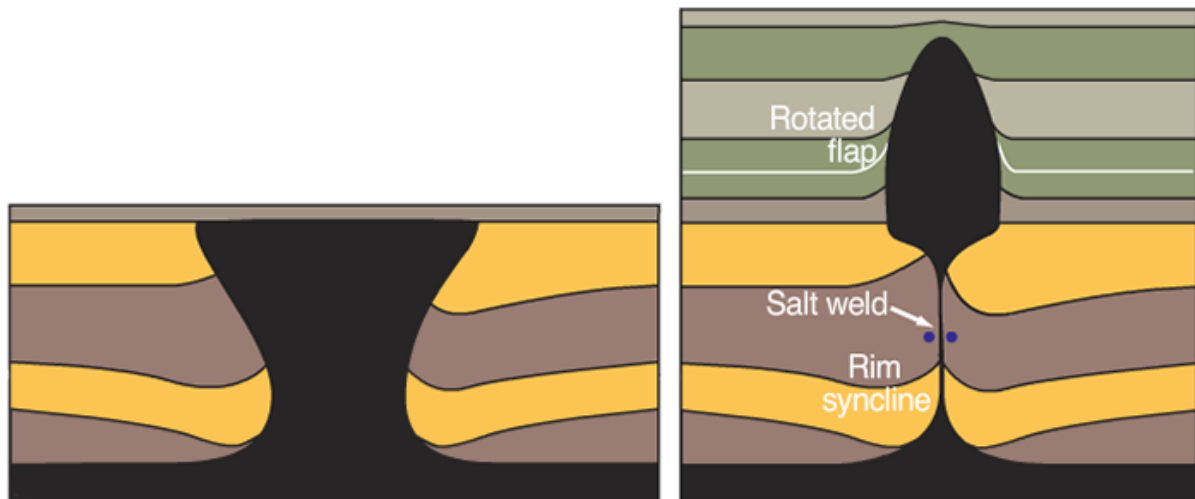


Figure 4 Uplift of a diapir in a compressional regime.

2 Utilization of salt rocks

Potash, halite and other salt types are mainly used in agriculture, but also important as raw material in chemistry, e.g. for the production of:

- soda lye, potash lye, muriatic acid; elements Na, K, Mg, Cl and Br (bromine)
- potash, saltpetre, soda, Glauber salt
- alkyl chlorides for the production of plastics and synthetic fibres
- washing powder, synthetic dyes, explosives
- additives for the textile, paper, leather, chemical pulp, oil, metallurgical, pharmaceutical and photochemical industry
- table salt, cooking salt, defrost salt and salt for fishing industry

The content of K^+ - ions is often used to compare and evaluate, respectively, the salt. The corresponding reference value is called K_2O content. E.g. the mineral sylvite has a content of 63 % and carnallite 17 % (D'Ans & Lax, 1967).

3 General behaviour

The mechanical behaviour of halite as a polycrystalline solid-state body depends on properties of the crystals and the grain boundaries. Plastic deformation develops within grains by dislocations, which are a result of translations within lattice areas of the most densely occupied lattice planes. To which extend the inter-crystalline or intra-crystalline processes govern the mechanical behaviour is highly dependent on acting stress, temperature and grain size. It is not possible to define a distinct yield point from which the plastic deformations start. One reason might be that in stress ranges with inactive inter-crystalline deformation processes, translations along grain boundaries dominate the deformation behaviour. Such a mechanism of plastic and viscose deformation within natural wet salt rocks is, for example, the pressure-solution creep, which governs the mechanical behaviour within stresses below about 10 MPa. Since the load exerted on load bearing elements (e.g. pillars) in salt mining is significantly higher, their strength- and deformation behaviour depends more on inter-crystalline processes at least within the pre-failure range. Consequently, the characteristic strength- and deformation behaviour within practical stress and load scenarios is primary a result of inter-crystalline processes and interactions.

Since salt rock formations are created under natural complex conditions (e.g. tectonic forces etc.) one has to consider that within a macroscopically homogeneous area the crystalline microstructure can be inhomogeneous, making it difficult to establish a representative analysis of the microstructure. Thus, the transformation of the microstructural behaviour to the deformation- and strength behaviour of load bearing elements or mining panels is connected with great uncertainties. Conversely, it is possible to describe the mechanical behaviour on the basis of rock mechanical parameters like stress σ , deformation ε and deformation rate $\dot{\varepsilon}$. The corresponding material parameters are determined for elementary volumes and act as integral macroscopic parameters. Based on such an approach, it is possible to describe the integral rock mechanical behaviour independently of the local microstructure and to obtain reliable predictions, for example, for a stable dimensioning of load bearing elements as well as for the proof of barrier integrity.

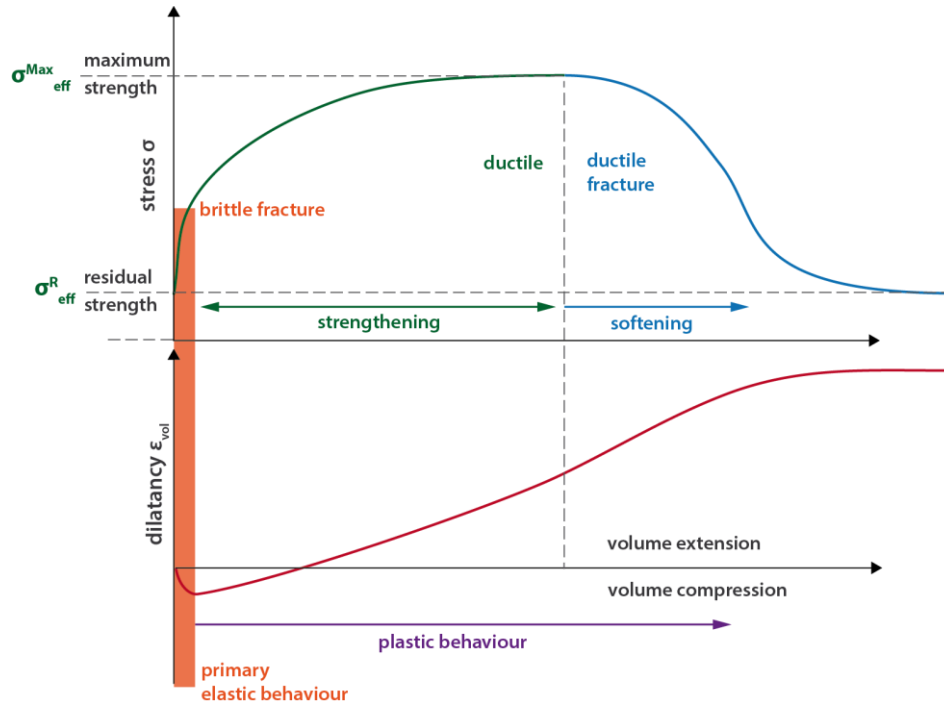


Figure 5 Characteristic stress-, deformation- and dilatation behaviour of halite under compressive stresses (deformation-controlled strength test); redrawn after Günther (2009).

Figure 5 illustrates the typical behaviour of a salt rock sample during a deformation-controlled strength test. During this test the sample experiences a compression by a constant deformation rate while measuring the stress. The measured total deformation is the sum of elastic (ε^{el}), thermal (ε^{th}), plastic (ε^p) and viscous (ε^v) components:

$$\varepsilon = \varepsilon^{el} + \varepsilon^{th} + \varepsilon^p + \varepsilon^v \quad (1)$$

In case of constant temperature the thermal deformation ε^{th} is zero, so that the total deformation is:

$$\varepsilon = \varepsilon^{el} + \varepsilon^p + \varepsilon^v \quad (2)$$

A distinct and characteristic behaviour of salt is the ability to creep, i.e. to show significant time-dependent plastic deformations. Due to the pronounced time dependence of the deformation it is not easy to distinguish between plastic and viscous deformation parts. Thus, the inelastic part of deformation is a combined visco-plastic deformation ε^{vp} .

$$\varepsilon = \varepsilon^{el} + \varepsilon^{vp} \quad (3)$$

In the following, ε^{vp} is set equal to the resulting deformation part ε_{cr} within the creep process.

Under high load rate, the elastic behaviour dominates within the lower stress range (Figure 5). It results from the deformation of a crystal lattice: although atoms are dislocated the bonds between the atoms remain intact. The deformation follows the applied load instantaneous and is completely reversible, i.e. the crystal lattice gains their former structures after unloading. With increasing load level the portion of non-reversible plastic deformation increases (Figure 5).

Plastic deformation which occurs before macroscopic failure is known as ductile and the ductility depends on the creep ability of a material, which is characterized by the viscosity.

Since the plastic deformation is related to an increase in volume (dilatancy) the point at which the plastic dilatancy $+\Delta\varepsilon_{\text{vol}}^{\text{pl}}$ equals the elastic volume compression $-\Delta\varepsilon_{\text{vol}}^{\text{el}}$ defines the beginning of the ductile range. In this range the plastic behaviour dominates (Figure 5). Within the ductile range the stress first increases with progressive deformation before failure occurs. This is due to the changes of the microstructure of the crystals, leading to a strain hardening of the material. In this case the failure is called ductile failure.

In salt rocks with pronounced ductile behaviour, the damage is accumulated during creep and can be directly determined by measuring the dilatancy during strength tests (Figure 5). Since the brittle failure develops during the damage process the strength behaviour of ductile salt rocks is strongly related to creep until failure even in the post failure region. In contrast, if the macroscopic failure happens directly subsequently the elastic part, i.e. without any significant visco-plastic deformation, it is called brittle failure. This behaviour is characteristic for carnallite which is less able to creep compared to other salt rocks. Within the failure and post-failure range cracking occurs between or across grains so that disintegration or softening increasingly governs the plastic deformation along macroscopic fracture- and shear planes.

The material strength is reduced within the post-failure range until it reaches the residual strength. The residual strength results from the cohesive and frictional properties of the completely disintegrated material. During a creep test (constant load) three phases can be distinguished (Figure 6):

- I. primary creep – also known as transient creep
- II. secondary or stationary creep
- III. tertiary creep or creep failure

These three creep phases are closely related to each other and show transitions within intra-crystalline deformation processes.

The primary creep is characterized by high creep rates which rapidly decrease with progressive deformation. Dislocations within the crystal lattice are dominating. With ongoing deformation the potential for further dislocations or movements, respectively, is decreasing. During ongoing deformation new dislocations within the crystal lattice occur, leading to a growing dislocation density and subsequently to an increasing resistance against the deformation. Thus, for a further constant deformation rate higher load is needed (strengthening); or conversely, the deformation rate decreases in case of a constant load (transient creep). The growing strengthening of the material acts as counterpart to the dislocation recovery which describes the elimination of the existing dislocations.

From the interactions of both mechanism - strengthening versus recovery – the stationary creep phase evolves by reaching the same values for the dislocation rate and dislocation recovery rate. Now, both rates are balanced and the creep rate becomes constant.

If the damage progresses and related softening starts above the dilatancy threshold, the tertiary creep phase begins. This is connected with an accelerated creep rate and leads finally to creep failure.

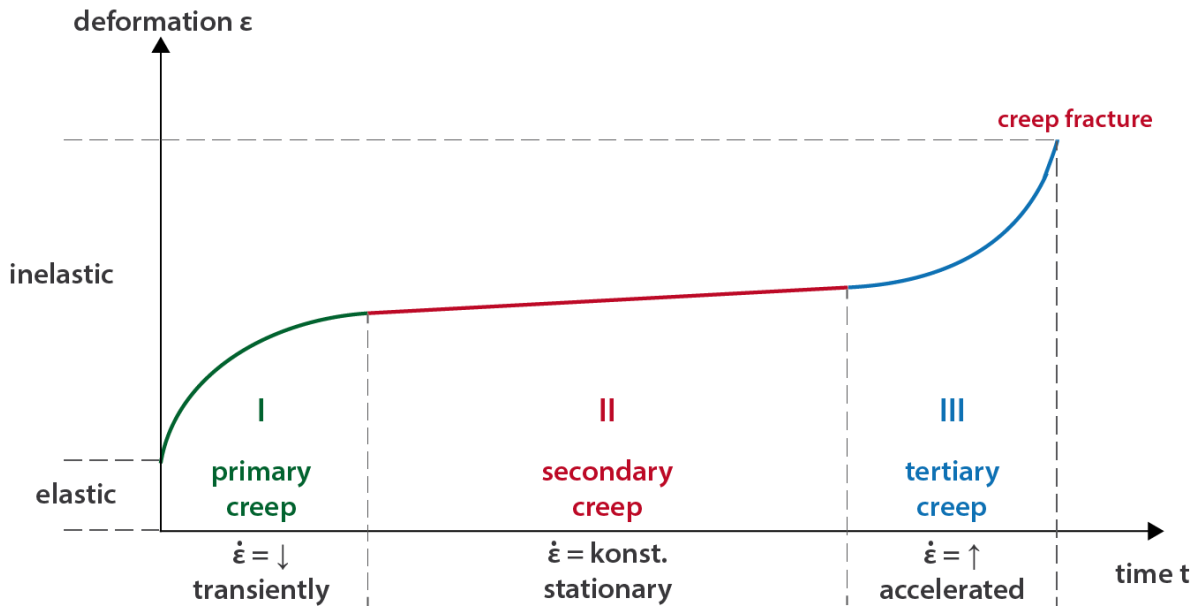


Figure 6 Creep test with three creep phases; redrawn after Günther (2009).

Primary and secondary creep can be fitted with reasonable accuracy by the so-called logarithmic creep law.

$$\varepsilon(t) = A + B \log t + Ct \quad (4)$$

Here the term A represents elastic deformation, the logarithmic term represents transient flow and the linear term represents steady-state flow (Odé, 1968). So the general formulation of time-dependent creep rate is given by the following equation.

$$\dot{\varepsilon}(t) = Bt^{-n} + C \quad (5)$$

4 Elastic behaviour

The elastic behaviour is described by Hooke's law. Elastic deformation occurs immediately after exerting load without any time delay. After unloading the deformations recover completely. Besides this reversible deformation the direct proportionality between stress and strain is characteristic for elastic material behaviour (Figure 7). The linear interrelationship between normal stress σ_{yy} and axial deformation ε_{yy} is described by the Young's modulus E (eq. 6). The relation between shear stress σ_{xy} and distortion angle γ_{xy} is expressed as shear modulus G (eq. 7).

$$\sigma_{yy} = E \cdot \frac{\Delta y}{y_0} = E \cdot \varepsilon_{yy} \quad (6)$$

$$\tau_{xy} = G \cdot \frac{\Delta x}{y_0} = G \cdot \varepsilon_{xy} \quad (7)$$

The relation between lateral strain ε_{xx} and axial strain ε_{yy} of a sample under uniaxial stress is called Poisson's ratio^V:

$$\nu = \frac{\varepsilon_{xx}}{\varepsilon_{yy}} \quad (8)$$

The elastic deformation is related to a volume change. Between isotropic pressure which corresponds to the octahedral normal stress σ_0 and the dilatancy ε_{vol} a linear interrelationship exist characterized by bulk modulus K .

$$\sigma_0 = \frac{(\sigma_{xx} + \sigma_{yy} + \sigma_{zz})}{3} = K \cdot \frac{\Delta V}{V_0} = K \cdot \varepsilon_{\text{vol}} \quad (9)$$

The elastic behaviour of an isotropic material can be completely expressed by the aforementioned parameters E , K , G and ν . In reality, only two of these parameters are necessary because the others can be mutually converted. Eq. 10 and eq. 11 show the relations between these four elastic constants:

$$G = \frac{E}{2 \cdot (1 + \nu)} \quad (10)$$

$$K = \frac{E}{3 \cdot (1 - 2\nu)} \quad (11)$$

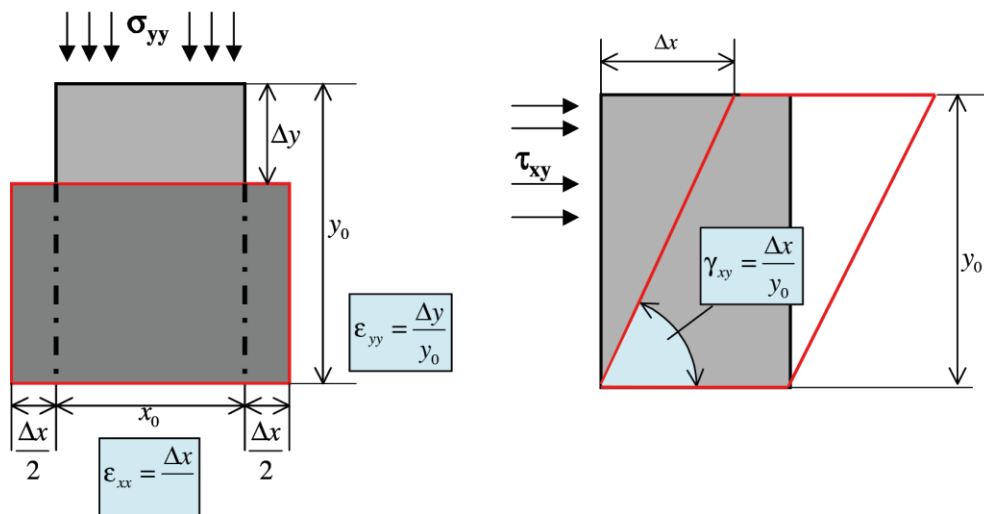


Figure 7 Elastic deformation of a sample (see also eq. 6 and eq. 7) (Günther, 2009).

5 Visco-plastic behaviour

This chapter, based on Günther (2009), describes the most important processes which occur during the ductile deformation of salt rocks. It involves the alteration of the micro-structure and describes the macroscopic behaviour of salt rocks.

In contrast to ideal crystals, the crystal lattice of real crystals contain defects (defects of the lattice geometry or periodic order of the atoms within the crystal). Lattice defects have a great influence on the deformation behaviour of real crystals. In accordance to the spatial extension in the crystal lattice the following defects can be distinguished:

Point defects describe defects that occur at or around a single lattice point. They have no spatial extensions in any dimension.

Two types of **one-dimensional or line defects** can be distinguished: **edge dislocation** and **screw dislocation**. They are caused by the disturbance of the lattice symmetry over several lattice planes in one direction. The direction and magnitude of the distortion is expressed in terms of the Burgers vector. In case the Burgers vector is perpendicular to the dislocation line we call it edge dislocation; conversely, if the Burgers vector is parallel to it we have a screw dislocation.

Two-dimensional or plane defects occur in two spatial directions over several lattice planes. Examples are grain- or phase boundaries. Grain boundaries occur where the crystallographic direction of the lattice abruptly is tilted or distorted. In case the tilted angle is $< 15^\circ$ it is called sub-grain. Phase boundaries separate crystal ranges of different chemical composition.

Three-dimensional defects or bulk defects comprise pores, micro-cracks and inclusions.

The ductile-plastic deformation of polycrystals and salt rocks is mainly based on the movement and development of dislocations. For the dislocation motion only few chemical bonds have to be detached at the same time so that the dislocation concept could reasonably explain the obvious low yield points of real crystals. During load above the yield point the material behaves ductile. In this case, not the complete lattice planes are displaced but rather local dislocations occur, migrating through the lattice as shown in Figure 8. Dislocation migration through the whole crystal leads to a deformation until it reaches barrier like grain boundaries, other dislocations or impurities.

The dislocation motion within a sliding plane (Figure 8) is known as dislocation sliding. If the dislocation does not move within the sliding plane, it is called dislocation climbing. The number of existing dislocations within a crystal is characterized by the dislocation density, which is a result of the relation between total length of the dislocation to crystal volume. In case of a low dislocation density, strength is close to the theoretical strength. With increasing dislocation density, plastic deformation starts already at low load levels. On the other hand, with growing dislocations, the motion of free dislocations is increasingly hindered, leading to material strengthening.

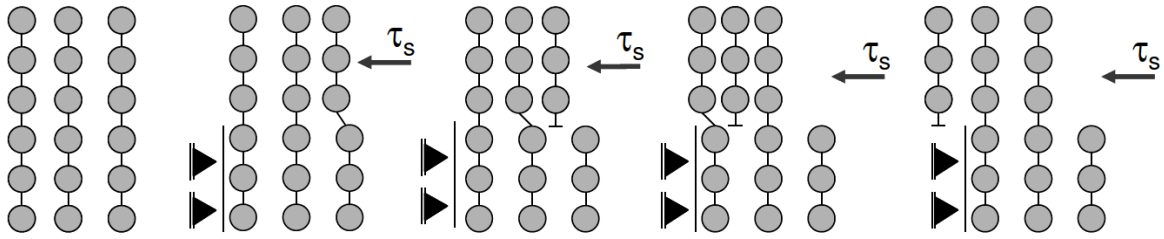


Figure 8 Dislocation mechanism (Günther, 2009).

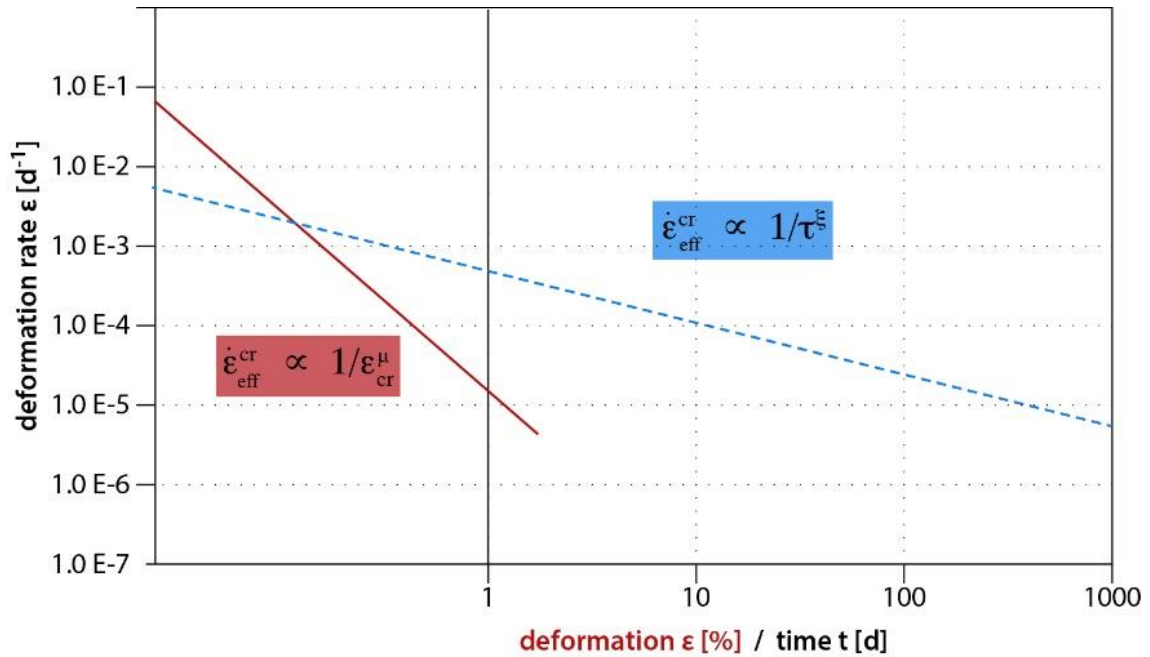


Figure 9 Deformation versus time (above) and Deformation rate versus deformation and time (below) at constant stress (classical creep test) (Günther, 2009).

Strain hardening

Let us assume a salt rock sample under constant compression with a constant deformation rate ($\dot{\epsilon} = \text{const.}$). As shown in Figure 5 the stress is growing within the inelastic-ductile pre-failure range. This process results from the intra-crystalline hardening of the sample which develops together with the visco-plastic deformation ϵ_{cr} as also shown in Figure 9 for a classical creep-test ($\sigma = \text{const.}$). During a creep test the hardening leads to a continuous reduction of the deformation rate $\dot{\epsilon}$.

The real structure of salt crystals, including lattice defects, depends on the conditions during the geological genesis and tectonic environment. The crystal grains (size, shape), the impurities by foreign phases and ions are structural and natural components. They influence the strengthening process directly by hindering the dislocation motion which leads to a dislocation blockade. Within the blocked area the dislocation motion is additionally blocked so that a growing load or force is needed to maintain the dislocation sliding (Wagner, 1999; Hahn, 2003; Günther, 2009).

In polycrystals grain boundaries act as additional dislocation barriers. For example, natural halite contains impurities in form of anhydrite phases. These finely distributed particles can also act as dislocation barriers, depending on their size and distribution. Hunsche (1996) investigated the influence of the microstructure on the creep behaviour of halite and showed that number and distribution of anhydrite phases strongly influence the strength- and deformation properties of halite. The higher the plastic deformation the stronger the blocking of dislocations.

Since the crystal lattice is distorted by dislocations, local elastic stress exists close to these dislocations. With growing dislocation density, the distance between the single dislocations is decreasing so that local stress fields of the single dislocations influence each other more and more by hindering the dislocation motion. The smaller the distance of dislocations the higher the force needed for triggering sliding \rightarrow strengthening (Wagner, 1999). Dislocations within one sliding plane therefore act as barriers for the dislocation within other sliding planes.

Since the increasing strength by means of migration of dislocations is directly coupled to the deformation, this process is also called deformational or extensional hardening. The dislocation density is an inner state variable of the crystalline microstructure which changes with plastic deformation. Thus, the material strength can be mathematically described by the dislocation density or plastic deformation. The relation between these variables is shown in Figure 9, which shows the time-dependent deformation behaviour of halite under constant load. Under these test conditions, with increasing visco-plastic deformation ε_{cr} , growing material hardening leads to a continuous reduction of the creep rate $\dot{\varepsilon}_{cr}$. For constant loads the relation between deformation and deformation rate is illustrated in Figure 9. In this relation, the proportionality factor A_p characterises the viscosity. The parameter μ describes the non-linearity:

$$\dot{\varepsilon} = f(\varepsilon_{cr}) = \frac{A_p}{(\varepsilon_{cr})^\mu} \rightarrow \sigma_{eff} = \text{const.} \quad (12)$$

Considering different stresses, eq. 12 has to be extended by a stress function $g(\sigma_{eff})$ to describe the extension-hardening-approach in a general form:

$$\dot{\varepsilon}_{cr} = f(\varepsilon_{cr}) \cdot g(\sigma_{eff}) \quad (13)$$

Nadai (1938) suggested to apply a power law for the stress dependency. Therefore, eq. 14 is used to describe the strain hardening behaviour of salt rocks at the macroscopic scale (Odqvist & Hult, 1962). The exponent n_p determines the characteristic non-linear stress dependency for the creep rate of rock salt.

$$\dot{\varepsilon}_{cr} = \frac{A_p}{(\varepsilon_{cr})^\mu} \cdot \sigma_{eff}^{n_p} \quad (14)$$

With increasing deformation the deformation rate is decreasing or additional load must be applied to maintain a constant deformation rate. The total visco-plastic deformation can be considered as an inner structural parameter which describes the state of hardening. Thus eq. 14 is a state equation (Odqvist & Hult, 1962) which illustrates the microstructural hardening at the macroscopic scale.

In contrast to the deformation-hardening (eq. 14) we can consider also time-dependent hardening as given by eq. 15 (Odqvist & Hult, 1962):

$$\dot{\varepsilon}_{cr} = \frac{A^*}{t^{\xi}} \cdot f(\sigma_{eff}) \quad (15)$$

The approach of eq. 15 is suitable to describe the behaviour under constant load or stress. The proportionality factor A^* is the rate of viscosity. Note, that relations given above are only valid for $\sigma_{eff} = \text{const.}$

Dislocation recovery

The material hardening developed during plastic deformation is limited by a process called recovery. After Blum (1978), the recovery comprises all dislocation reactions which counteract the hardening. Due to plastic deformation the number of dislocations grows and they interfere each other. This strengthening process leads to a growing internal energy of the material, producing a more and more instable dislocation structure. The recovery reduces this internal energy by eliminating or rearranging the dislocations to an energetic more favourable state (Hahn, 2003). The dislocations are re-orientated and network-like structures develop and form so-called sub-grains. Dislocations within this sub-grains migrate towards sub-grain boundaries by dislocation sliding. The dislocation density within the sub-grains will be reduced and; conversely, increased at the sub-grain boundaries (Blum, 1978). Since differently orientated dislocations are pulling against each other in areas of high dislocation density, the probability of eliminating dislocations by annihilation increases (Fokker, 1998). During this process, dislocations with different orientations will be eliminated if they lie within one sliding plane and unit (Figure 10).

Since screw dislocations have no distinct sliding planes they can migrate by crosswise sliding. Blocked edge dislocations (Figure 11a) can change the sliding plane by climbing. During this mechanism those dislocations, which do not contribute to the outer stress field due to their spatial orientation, produce zero-dimensional vacancies. These point defects move to blocked edge dislocations by diffusion and become attached to them (Elliger, 2005), which change the structure of the formerly blocked dislocations and enables again dislocation sliding (Figure 11b). The vacancy diffusion becomes faster at higher temperature. Accordingly, the recovery mechanism is based on the climbing and crosswise sliding of dislocations so that dislocations within different sliding planes can switch among them to become unified or eliminate each other (Figure 11c). The recovery is a thermally activated process which is based on the interactions between the different dislocations and counteracts against the development of dislocations.

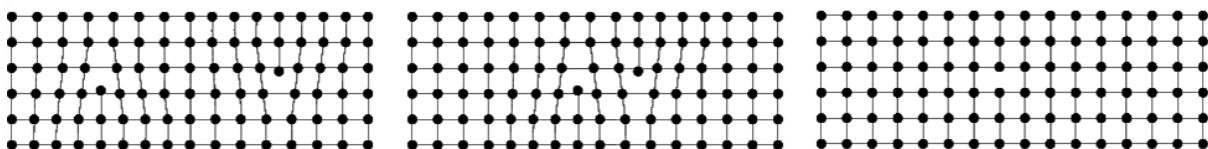


Figure 10 Elimination and dislocation of one sliding plane by annihilation.

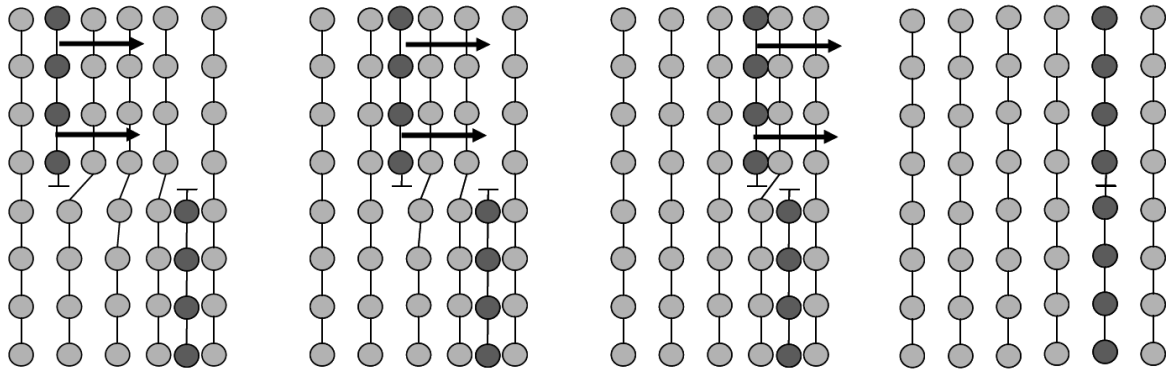


Figure 11 Dislocation climbing and annihilation (Günther, 2009).

Under consideration of the recovery the development of the dislocation structure can be expressed as:

$$\dot{\rho} = \dot{\rho}^+ - \dot{\rho}^- \quad (16)$$

where $\dot{\rho}$ is the alteration rate of the dislocation density and $\dot{\rho}^+ - \dot{\rho}^-$ is the difference between rate of generation and rate of elimination (Blum, 1978).

The total visco-plastic deformation $\dot{\varepsilon}_{cr}$ is a result of all dislocation reactions. Their rates comprise the part of hardening $\dot{\varepsilon}_{cr}^V$ and the part of recovery $\dot{\varepsilon}_{cr}^E$ (eq. 17).

$$\dot{\varepsilon}_{cr} = \dot{\varepsilon}_{cr}^V + \dot{\varepsilon}_{cr}^E \quad (17)$$

Re-arranging of eq. 17 leads to eq. 18, which is of same type like eq. 16 (Salzer, 1993):

$$\dot{\varepsilon}_{cr}^V = \dot{\varepsilon}_{cr} - \dot{\varepsilon}_{cr}^E \quad (18)$$

Both, eq. 16 and eq. 18, describe the nature of ductile deformation of crystalline solid bodies. In contrast to eq. 16, eq. 18 describes the creep at the macroscopic scale.

Since the macroscopic creep is a result of the motion and generation of dislocations also the macroscopic creep rate $\dot{\varepsilon}_{cr}$ is a result of $\dot{\rho}^+$ which generates the dislocations within internal volume elements. The internal elimination rate $\dot{\rho}^-$ also causes external deformation which is described by means of the recovery rate $\dot{\varepsilon}_{cr}^E$.

Analog to eq. 16, eq. 18 is part of the deformation rate $\dot{\varepsilon}_{cr}^V$ from which the hardening comes from - as result of the balance between $\dot{\varepsilon}_{cr}$ and $\dot{\varepsilon}_{cr}^E$.

In case the total viscose deformation $\dot{\varepsilon}_{cr}$ in eq. 14 is replaced by the deformation part $\dot{\varepsilon}_{cr}^V$, it is also possible to consider the crystal recovery within the extension-hardening approach in accordance to eq. 19. In this case, primary and secondary creep are described in a coupled manner (Salzer, 1993).

$$\dot{\varepsilon}_{cr} = \frac{A_p}{(\varepsilon_{cr}^V)^\mu} \cdot \sigma_{eff}^{n_p} \quad (19)$$

As long as the hardening part of the deformation ε_{cr}^V is positive, the deformation is within the transient phase. Since the hardening- and recovering processes strive for equilibrium, rates of generation and elimination of dislocations becomes equal. Consequently, the rate of the hardening part of ε_{cr}^V tends towards zero. Within this state, the microstructure of the material remains stable so that the resistance against deformation does not alter under constant load (Blum, 1978). Therefore, at the macroscopic scale it means that the rate of deformation remains constant under constant stress and temperature and the material enters the secondary creep phase.

Damage and Dilatancy

Microcracks, pores etc. always exist and can grow during visco-plastic deformation. Damage development is related to hardening (Figure 12). In salt rocks the generation of microcracks is related to a volume increase, also called volumetric deformation ε_{vol} , dilatancy or volume dilatancy. In ductile salt rocks the dilatancy starts with the beginning of the visco-plastic hardening under load levels which are far below the short-term strength. Figure 13 shows the behaviour of a salt rock sample under deformation-controlled triaxial conditions. It documents the mutual influence of dilatancy and strength. Hardening and softening compensate each other at peak strength, so that the slope of the stress curve becomes zero (perfect plasticity). In contrast, the material becomes progressively softened in the post-failure range which is related to a disproportionally increase of the volume expansion. Besides the development of micro cracks within the range of dislocation blocking, also local tensile failure can contribute to the volume dilatancy in ductile salt rocks. Both softening processes interfere with each other and, therefore, the dilatancy can be considered as an integral measure for the state of softening.

Due to its pronounced ability to creep the strength behaviour of salt rocks is quite different from rocks without this ability. Normally, the strength behaviour of rocks is analysed by triaxial tests, exerting axial load on a sample at different confining pressures under deformation-controlled conditions with relative high rates of deformation in the order of $1 \cdot 10^{-5} \text{ s}^{-1}$ to $3 \cdot 10^{-5} \text{ s}^{-1}$. These tests include also the post-failure range. The deformation behaviour analysed on the basis of triaxial tests highly depends on the loading rate. With decreasing deformation rate the peak strength decreases and the deformation in the pre-failure range increases. That means, that for salt rocks: one has to distinguish between higher short-term strength (determined under high loading rates) and reduced long-term strength under reduced loading rates. To consider this behaviour for pillar dimensioning in mining, Menzel & Schreiner (1977) introduced a rheological safety factor, describing the expected stand-up time in dependence on the degree of utilization of the short term strength.

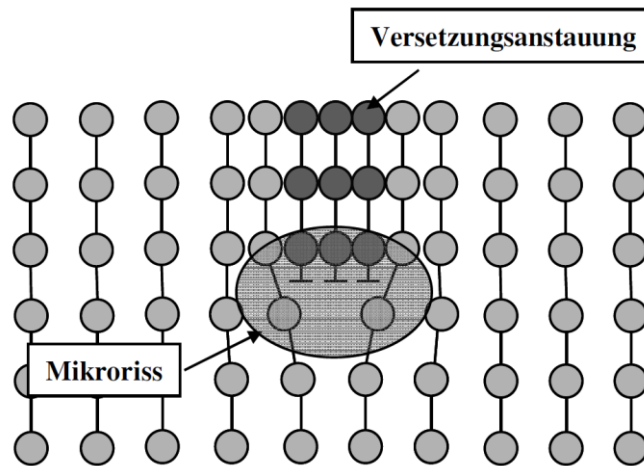


Figure 12 Development of microcracks in the area of built-up dislocations (Günther, 2009).

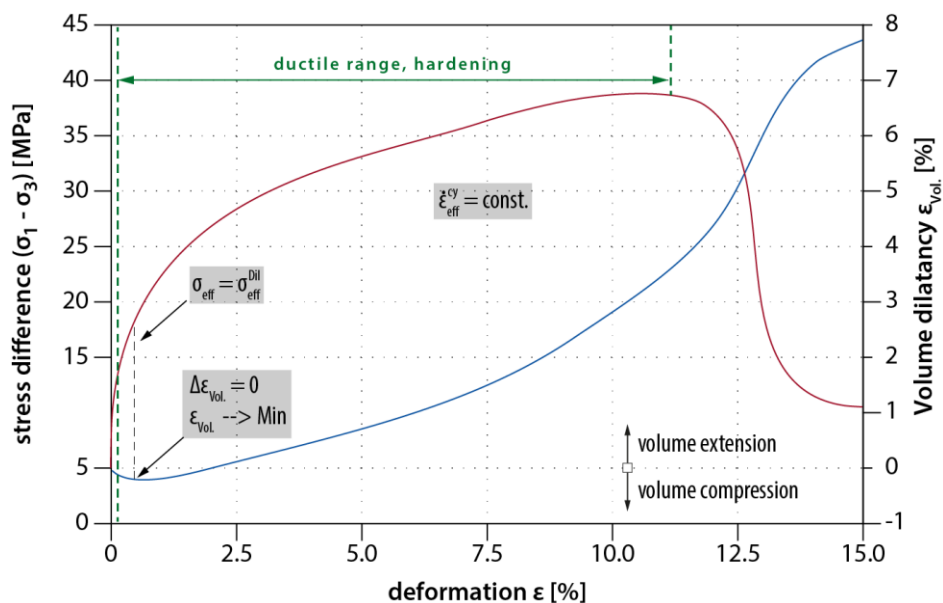


Figure 13 Sketch of strength (red) and dilatancy (blue) development in a deformation-controlled triaxial test; redrawn after Günther (2009).

The calculation of the rheological safety factor is based on the assumption that within a defined mechanical state, the salt rock can absorb a certain amount of energy without loosening its strength. The specific dissipation energy of a solid body, i.e. the work of the internal forces per volume- and time-unit is:

$$\dot{U} = \sigma_{ij} \cdot \dot{\varepsilon}_{ij} \quad (20)$$

The specific work during creep deformation is given by:

$$U = \int_0^t \sigma_{\text{eff}} \cdot \dot{\varepsilon}_{\text{cr}} dt \quad (21)$$

Menzel & Schreiner (1977) described the transition from short-term to long-term strength of halite in dependence on the specific strain energy. A proceeding deformation leads to

hardening but the increasing development of micro cracks counteracts. A complete deformation-hardening without recovery leads to a relatively high hardening but also to a reduction of the damage-free deformation reserve. With decreasing deformation rates or longer stand-up time, respectively, the process of dislocation recovery becomes increasingly important: blocked dislocations are being reactivated by dislocation climbing causing an increase in deformability or ability to creep, resp. A crucial factor hereby is that the recovery itself does not cause damages but rather contributes to the decrease of inter-crystalline stress by dislocation annihilation and thus counteracts against the development of micro cracks. This leads to a reduced accumulation of micro cracks during low deformation rates resulting in higher total deformation or longer stand-up time before failure occurs. If the micro crack density reaches a critical value, failure can occur also at low stresses. Thus, for the strength of salt rock the acting stress and state of deformation as described by Menzel & Schreiner (1977) have to be considered within the framework of the specific strain energy.

The state of stress measured at the onset of dilatancy is known as dilatancy limit $\sigma_{\text{eff}}^{\text{Dil}}$ (Figure 13). It is difficult to determine this point exactly because elastic volumetric compression and plastic volumetric dilatancy are overlapping processes and occur simultaneously. At the minimum of the dilatancy curve, the decrement of the elastic volume compression is identical with the increment of the plastic volume dilatancy. Therefore, the plastic volume dilatancy already starts before the minimum of the dilatancy is reached. This is confirmed by results of ultrasonic wave measurements on samples which have shown that V_s changes significantly close to the minimum of the dilatancy curve due to beginning micro crack development (Popp, 2002; Hunsche & Schulze, 2003). Hunsche introduced the term of micro crack limit which marks the onset of the damage development. As dilatancy limit he defined a plane in the stress space at which the volumetric extension rate is zero. Accordingly, the dilatancy limit is defined by the minimum of the dilatancy curve. Experimental investigations showed that the onset of dilatancy in the vicinity of this limit is slow. In fact, a discrimination between the compressive and dilatant stress range is vague (Hunsche & Hampel, 1999), so that different authors define different dilatancy limits.

The practical importance of the dilatancy limit is that in each rock whose state of stress is beyond this limit damage will be accumulated leading to failure in a long-term. Thus, the dilatancy limit is important for long-term stability considerations.

6 Constitutive models for salt rocks

There are different approaches to describe the behaviour explained in the chapters before. The total creep rate always contains primary and secondary parts ($\dot{\varepsilon}_{\text{cr}}^{\text{p}}$, $\dot{\varepsilon}_{\text{cr}}^{\text{s}}$), either with or without a damage part $\dot{\varepsilon}_{\text{cr}}^{\text{d}}$:

$$\dot{\varepsilon}_{\text{cr}} = f(\dot{\varepsilon}_{\text{cr}}^{\text{p}}, \dot{\varepsilon}_{\text{cr}}^{\text{s}}, \dot{\varepsilon}_{\text{cr}}^{\text{d}}) \quad (22)$$

The primary creep $\dot{\varepsilon}_{\text{cr}}^{\text{p}}$ is also called transient creep. The creep deformation ε_{cr} is related to the effective stress σ_{eff} . The corresponding creep deformation rate is given by:

$$\dot{\varepsilon}_{ij}^{cr} = \frac{3}{2} \dot{\varepsilon}_{cr} \cdot \frac{S_{ij}}{\sigma_{eff}} \quad (23)$$

Effective (equivalent) deformation and stress (ε_v , σ_v) are defined as follows (Backhaus, 1983):

$$\begin{aligned} \varepsilon_{eff} = \varepsilon_v &= \sqrt{\frac{2}{3} \sum_{ij} \varepsilon_{ij}^2} \\ \sigma_{eff} = \sigma_v &= \sqrt{\frac{3}{2} \sum_{ij} S_{ij}^2} \end{aligned} \quad (24)$$

Where $S_{ij} = \sigma_{ij} - (1/3)\sigma_{kk}\delta_{ij}$ and $\sigma_{kk} = \sigma_{11} + \sigma_{22} + \sigma_{33}$.

$\dot{\varepsilon}_{cr}$ basically depends on the effective stress σ_{eff} , the temperature T , a structural parameter V which describes the hardening and a structural parameter D which describes the damage.

$$\dot{\varepsilon}_{cr} = f(\sigma_{eff}, T, V, D) \quad (25)$$

For the description of the temperature dependency of $\dot{\varepsilon}_{cr}$ very often the Arrhenius term is applied (eq. 26), which is multiplicatively related with the stationary creep rate $\dot{\varepsilon}_{cr}^s$.

$$f(T) = e^{\left(-\frac{Q}{R \cdot T}\right)} \quad (26)$$

In the Arrhenius term R is the universal gas constant with 8.314 J/(mol K), T is the acting absolute temperature ($[T] = K$) and Q is the activation energy for the creep process ($[Q] = J/mol$). The activation energy Q is temperature-dependent and increases non-linear with increasing temperature. In modelling, the assumption of a mean activation energy $Q = 54$ kJ/mol in relation with eq. 26 is very common. This approach describes the temperature-dependency of the creep generally with an accuracy which is sufficient for most practical tasks.

The actual creep phase of the material depends on the actual state of the microstructure. As long as the crystalline structure is changing also the deformation properties change, leading to primary or transient creep, resp., or to a damage induced softening. Within a microstructural balance in case the structure does not change, also the deformation properties remain constant, resulting in a secondary or stationary creep, resp. The transition from a changing to a stationary microstructure is continuously and depend on whether the dislocations are eliminated or new ones are created. In material modelling, this process can be described by means of a corresponding structural parameter, which becomes a constant during secondary creep. Material models without such a hardening parameter can only describe a secondary creep but not the transient creep. Since the microstructure of salt rocks always strives to reach a stationary state, these simple material models are generally an important basic component of all complex material approaches. In the following sections a few popular constitutive models for salt creep are given.

1.1 Basic Models

- **time-dependent strengthening model**

Based on the logarithmic creep law given in eq. 5 and eq. 6 Boresi & Deere (1963) developed a time-dependent strengthening model for the transient creep phase (Lux, 1984; Hou, 1997) with stress exponent n , time exponent m and a material constant a (eq. 27). Typical values are shown in This law describes the permanent decrease of the creep rate which is typical for transient creep. It also considers the non-linear stress dependency.

$$\dot{\varepsilon}_{cr}^p(t) = m \cdot a \cdot \sigma_{eff}^n \cdot t^{m-1} \quad (27)$$

This law describes the permanent decrease of the creep rate which is typical for transient creep. It also considers the non-linear stress dependency.

- **strain hardening model**

Based on eq. 14 the **strain hardening model** (Menzel & Schreiner, 1975 - 1978) is used by many authors (Odqvist & Hult, 1962; Menzel & Schreiner, 1977; Salzer, 1993).

$$\dot{\varepsilon}_{cr}^p = A \cdot \frac{\sigma_{eff}^n}{(\varepsilon_{eff})^\mu} \quad (28)$$

Here ε_{eff} and $\dot{\varepsilon}_{cr}$ are the inelastic equivalent deformation and deformation rates respectively (see also Table 3). Within this constitutive law the transient creep rate is decreasing.

- **Norton power law**

The most common expression to describe the stress, temperature and micro-structure dependence of the steady-state creep rate is based on the **Norton power law** (Norton, 1929) and the Arrhenius term

$$\dot{\varepsilon}_{cr}^s = A \cdot e^{\left(\frac{-Q}{RT}\right)} \cdot \sigma_{eff}^n, \quad (29)$$

where $\dot{\varepsilon}_{cr}^s$ is the stationary creep rate without elastic parts. Factor A and exponent n are material parameters (Table 4 Typical values for the Norton power law Table 4).

- **simplified Norton power law**

For constant temperature the **simplified Norton power law** is an often-used approach for steady-state creep rate.

$$\dot{\varepsilon}_{cr}^s = \bar{A} \cdot \sigma_{eff}^n \quad (30)$$

In this case factor \bar{A} includes the temperature-dependency. This approach can only be used if \bar{A} is known or determined (Table 5).

Table 2 Typical values for the time dependent strengthening model after Boreis & Deere (1963)

Parameter	n	m	a
Value	5	0.12	$3.9 \cdot 10^{-9}$

Table 3 Typical values for the strain hardening model (Hou, 1997)

Parameter	μ	n	A
Value	2 ... 7	9 ... 15	$10^{-34} \text{ d}^{-1} \dots 10^{-21} \text{ d}^{-1}$

Table 4 Typical values for the Norton power law (Schoenherr, Schléder, Urai, Fokker, & Schulze, 2007)

Parameter	A	Q	n
Value	$10^{-6} \text{ s}^{-1} \dots 10^{-3} \text{ s}^{-1}$	25 kJ/mol ... 80 kJ/mol	3 ... 6

Table 5 Typical values for the simplified Norton power law (Hou, 1997)

Parameter	\bar{A}	n
Value	$10^{-12} \text{ s}^{-1} \dots 10^{-9} \text{ d}^{-1}$	3 ... 5

Table 6 Typical values for the BGR_a constitutive model (Hou, 1997; Günther, 2009)

Parameter	Q	n_s	σ_0 (ref. stress)	A_s
Value	54 kJ/mol	5	1 MPa	0.18 d^{-1}

Table 7 Typical values for the BGR_b constitutive model (Hou, 1997)

Parameter	A_{s1}	A_{s2}	n_s
Value	$2.3 \cdot 10^{-4} \text{ d}^{-1}$	$2.1 \cdot 10^{-6} \text{ d}^{-1}$	5

- **BGR_a constitutive model**

The BGR_a constitutive model (Hunsche & Schulze, 1994) is using a potential approach for the stationary creep phase. It was used to describe the temperature dependency of the „Asse“ salt rock for a temperature range between 22 °C to 200 °C assuming a constant mean activation energy of $Q = 54 \text{ kJ/mol}$ (Table 6).

$$\dot{\varepsilon}_{cr}^s = \left[A_s \cdot e^{\left(\frac{-Q}{R \cdot T}\right)} \right] \cdot \left(\frac{\sigma_{eff}}{\sigma_0} \right)^{n_s} \quad (31)$$

- **BGR_b constitutive model**

The BGR_b constitutive model (Hunsche & Schulze, 1994) is an extension of the BGR_a model and uses a bipartite Arrhenius-term in which two different activation energies are specified. For the salt dome Gorleben, Hunsche & Schulze (1994) defined two activation energies: $Q_1 = 42 \text{ kJ/mol}$ ($T < 100 \text{ °C}$) and $Q_2 = 113 \text{ kJ/mol}$ ($T > 100 \text{ °C}$) (Table 7).

$$\dot{\varepsilon}_{cr}^s = \left[A_{s1} \cdot e^{\left(\frac{-Q_1}{R \cdot T}\right)} + A_{s2} \cdot e^{\left(\frac{-Q_2}{R \cdot T}\right)} \right] \cdot \left(\frac{\sigma_{eff}}{\sigma_0} \right)^{n_s} \quad (32)$$

1.2 Basic rheological models

The modelling of the creep behaviour by means of rheological models corresponds to the phenomenological description of the deformation behaviour (e.g. elasticity, plasticity, viscosity ...) without relating to the responsible deformation mechanism. The occurring elastic, plastic and viscose deformation parts are described by a spring, a friction block and a dashpot. Within material models for salt rocks without damage and failure, the following deformation parts have to be distinguished:

- elastic isotropic compression ε^{el} - **spring element (Hooke element)**: time-independent reversible (see Figure 14).

$$\varepsilon_{ij}^{el} = \frac{1}{2G} \cdot \left(\sigma_{ij} - \frac{\nu}{1-\nu} \cdot \sigma_{kk} \cdot \delta_{ij} \right) \quad (33)$$

- elastic transient deformation part ε^{ve} - **Kelvin element**: time-dependent, reversible

$$\dot{\varepsilon}_{ij}^{ve} = \frac{1}{2\eta_K} \cdot S_{ij} - \frac{G_K}{\eta_K} \cdot \varepsilon_{ij}^{ve} \quad (34)$$

For definition of stress deviator S_{ij} see page 18. In a similar way the strain deviator e_{ij} is defined: $e_{ij} = \varepsilon_{ij} - (1/3)\varepsilon_{kk}\delta_{ij}$ and $\varepsilon_{kk} = \varepsilon_{11} + \varepsilon_{22} + \varepsilon_{33}$.

- visco-plastic deformation part ε^{vp} - **Maxwell element**: time-dependent, irreversible

$$\dot{\varepsilon}_{ij}^{vp} = \frac{1}{2G_M} \cdot \dot{S}_{ij} + \frac{1}{2\eta_M} \cdot S_{ij} \quad (35)$$

The total deformation is the result of the superposition principle of the different deformation parts:

$$\varepsilon = \varepsilon^{el} + \varepsilon^{ve} + \varepsilon^{vp} \quad (36)$$

The serial connection of the Kelvin- and Maxwell-model leads to the phenomenological

rheological **Burgers model**. In combination with the Hooke element it depicts a rheological basic model for the creep behaviour of salt rocks.

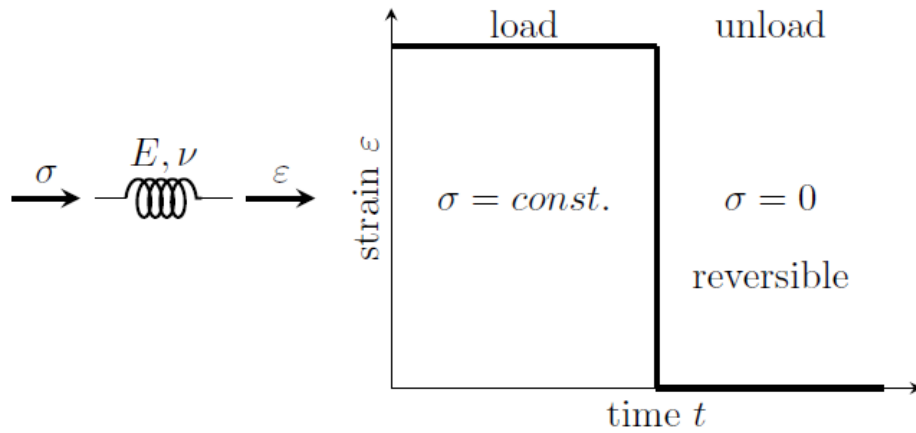


Figure 14 Hooke element: scheme and deformation during loading and unloading

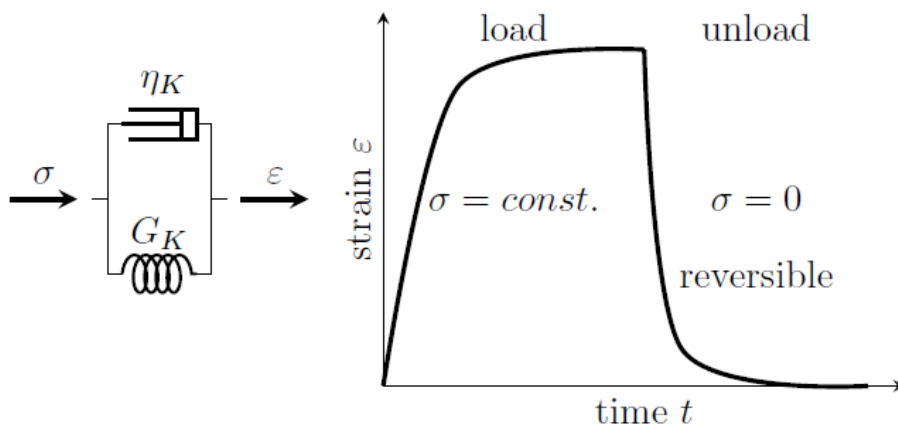


Figure 15 Kelvin model: scheme and deformation during loading and unloading

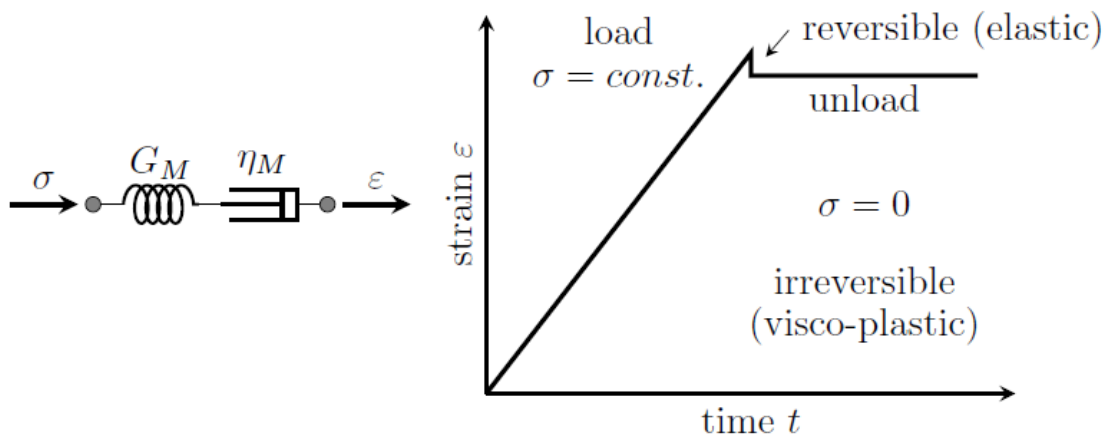


Figure 16 Maxwell model: scheme and deformation during loading and unloading

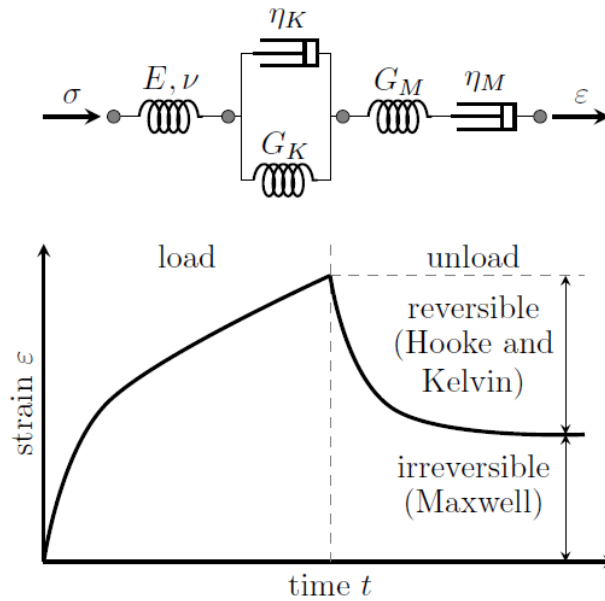


Figure 17 Burgers model: Rheological basic model for creep behaviour of salt rocks

The Kelvin-model provides the complete reversible deformation part as primary deformation during elastic transient load. Together with the Maxwell model it provides an undamaged irreversible visco-plastic deformation part. The Burgers-model describes the linear dependency between the secondary creep rate and the exerting stress. Since such a linear relation doesn't exist for salt rocks several other models or modification, resp., were developed.

1.3 Advanced and complex models

- **time-dependent creep-damage model**

This model (Wang, 2004) includes primary and secondary creep as well as an easy approach to include tertiary creep.

$$\begin{aligned}\dot{\epsilon}_{cr} &= \dot{\epsilon}_{cr}^p + \dot{\epsilon}_{cr}^s + \dot{\epsilon}_{cr}^d \\ \dot{\epsilon}_{cr}^p &= \frac{\sigma}{C_1} \cdot \left[1 - e^{\left(-\frac{G}{C_2} t\right)} \right] \\ \dot{\epsilon}_{cr}^s &= A_1 \cdot e^{\left(-\frac{Q_1}{R \cdot T}\right)} \cdot \sigma^n \cdot t \\ \dot{\epsilon}_{cr}^d &= A_2 \cdot e^{\left(\frac{Q_2}{R \cdot T}\right)} \cdot \left(\frac{\sigma}{1-D}\right)^n \cdot t\end{aligned}\tag{37}$$

The advantage of this model is the low number of parameters. Typical values for low and high stress levels can be found in the original publication (Wang, 2004).

- **composite model / composite dilatancy model**

The composite model (Hampel, et al., 2007) describes primary and stationary creep. The model is based on considering the crystalline microstructure by means of structural components D_i with corresponding microscopic activation energy $Q = 180$ kJ/mol and internal effective stress σ^* :

$$\dot{\epsilon}_{cr} = f(D_i, \sigma) \cdot e^{\left(\frac{Q}{R \cdot T}\right)} \cdot \sinh\left(\frac{g(D_i) \cdot \sigma^*}{T}\right) \quad (38)$$

This model was further developed to the composite dilatancy model (CDM) including dilatancy influence on creep and softening process due to moisture spreading in structural failure.

- **MD model / MDCF model**

The MD model (Multimechanism Deformation) (Munson & Dawson, 1979; Munson & Dawson, 1984) describes dislocation creep based on microstructural deformation mechanisms, which are basically described in section 5. Stationary creep rate $\dot{\epsilon}_{cr}^s$ is the superposition of dislocation climbing term $\dot{\epsilon}_{cr}^{s1}$, a term from an undefined mechanism $\dot{\epsilon}_{cr}^{s2}$ and a term from dislocation sliding $\dot{\epsilon}_{cr}^{s3}$. In this model primary creep rate and stationary creep rate are multiplied to get total creep rate (for parameters see Table 8).

$$\begin{aligned} \dot{\epsilon}_{cr} &= \dot{\epsilon}_{cr}^p \cdot \dot{\epsilon}_{cr}^s = f(\sigma_{eff}, T) \cdot (\dot{\epsilon}_{cr}^{s1} + \dot{\epsilon}_{cr}^{s2} + \dot{\epsilon}_{cr}^{s3}) \\ \dot{\epsilon}_{cr}^{s1} &= A_1 \cdot e^{\left(\frac{Q_1}{R \cdot T}\right)} \cdot \left(\frac{\sigma_{eff}}{\mu}\right)^{n_1} \\ \dot{\epsilon}_{cr}^{s2} &= A_2 \cdot e^{\left(\frac{Q_2}{R \cdot T}\right)} \cdot \left(\frac{\sigma_{eff}}{\mu}\right)^{n_2} \end{aligned} \quad (39)$$

This model was further developed to the **MDCF model** (Multimechanism Deformation Coupled Fracture) including description of damage and recovery.

- **Lubby2 model / Hou/Lux model**

The Lubby2 model is a non-linear Burgers model (Hou, 1997) with terms of the Kelvin- and Maxwell-creep.

$$\begin{aligned} \dot{\epsilon}_{cr} &= \dot{\epsilon}_{cr}^K + \dot{\epsilon}_{cr}^M + \dot{\epsilon}_{cr}^p + \dot{\epsilon}_{cr}^s \\ \dot{\epsilon}_{cr}^p &= \frac{\sigma}{\eta_K} \left(1 - G_K \frac{\epsilon_{cr}}{\sigma_{eff}}\right) \\ \dot{\epsilon}_{cr}^s &= \frac{\sigma_{eff}}{\eta_M} \end{aligned} \quad (40)$$

In the Lubby2 model viscosities η_K , η_M and the shear modulus G_K are certain functions of σ_{eff} :

$$\begin{aligned} G_K &= G_K^* \cdot e^{(k_1 \cdot \sigma_{eff})} \\ \eta_K &= \eta_K^* \cdot e^{(k_2 \cdot \sigma_{eff})} \\ \eta_M &= \eta_M^* \cdot e^{(m \cdot \sigma_{eff})} \cdot e^{(l \cdot T)} \end{aligned} \quad (41)$$

This model was further developed to the Hou/Lux model with (MDS) or without (ODS) damage.

Table 8 Typical values for the Multimechanism Deformation model_(Hou, 1997)

Parameter	Value
A_1	$8.4 \cdot 10^{22} \text{ s}^{-1}$
Q_1	$1.04 \cdot 10^5 \text{ J/mol}$
n_1	5.5
A_2	$9.7 \cdot 10^{12} \text{ s}^{-1}$
Q_2	$4.18 \cdot 10^5 \text{ J/mol}$
n_2	5.0

Table 9 Typical parameter values for Lubby2 model (Hou, 1997)

Parameter	Value with temp. effect	Value without temp. effect
G_K^*	$10^4 \text{ MPa} \dots 10^5 \text{ MPa}$	
η_K^*	$10^4 \text{ MPa} \cdot \text{d} \dots 10^5 \text{ MPa} \cdot \text{d}$	
k_1	$-0.15 \text{ MPa}^{-1} \dots -0.25 \text{ MPa}^{-1}$	
k_2	$-0.15 \text{ MPa}^{-1} \dots -0.30 \text{ MPa}^{-1}$	
η_M^*	$10^{13} \text{ MPa} \cdot \text{d} \dots 10^{14} \text{ MPa} \cdot \text{d}$	$10^7 \text{ MPa} \cdot \text{d} \dots 10^8 \text{ MPa} \cdot \text{d}$
m	$-0.25 \dots -0.4$	$-0.25 \dots -0.4$
l	-0.05	0.00

- **Günther/Salzer model**

Based on the strain hardening model (Odqvist & Hult, 1962; Menzel & Schreiner, 1977) and the Norton power law the Günther/Salzer model (G/S) introduces an additional term, that arises from transient stress-dependence, to describe primary creep (Günther, et al., 2016).

$$\dot{\varepsilon}_{\text{cr}}^{\text{p}} = A_{\text{p}}(T, \sigma_{\text{eff}}) \cdot \frac{\sigma_{\text{eff}}^{n_{\text{p}}}}{(\varepsilon_{\text{str}} + \varepsilon_{\text{str},0})^{\mu}} \quad (42)$$

$$A_{\text{p}}(T, \sigma_{\text{eff}}) = \frac{e^{\left(\frac{Q_{\text{p}}}{R \cdot T}\right)}}{\frac{1}{A_{\text{p},R}} + \frac{1}{A_{\text{p},0}} \cdot e^{(-m_{\text{p}} \cdot \sigma_{\text{eff}})}}$$

Here $A_{\text{p},R}$ is the factor at high stresses, $A_{\text{p},0}$ is the factor at $\sigma_{\text{eff}} = 0$ and m_{p} is a curvature parameter. During the initial loading, deformation is dominated by dislocation motion, already applied within the crystal (initial strain hardening $\varepsilon_{\text{str},0}$).

η_p and μ are equivalent to parameters n and μ in eq. 28. In eq. 42 p denotes parameters for primary creep. The term A in eq. 28 is now stress- and temperature-dependent.

For stationary creep an approach is used, that consists of three single terms (Günther, et al., 2016).

$$\dot{\varepsilon}_{cr}^s = A_{s1} e^{\left(\frac{Q_1}{R \cdot T}\right)} \cdot \sigma_{eff}^{n_{s1}} + A_{s2} e^{\left(\frac{Q_2}{R \cdot T}\right)} \cdot \sigma_{eff}^{n_{s2}} + A_{s3} e^{\left(\frac{Q_3}{R \cdot T}\right)} \cdot \sigma_{eff}^{n_{s3}} \quad (43)$$

The terms ('s' denotes secondary creep) are based on the Norton power law (similar to BGR_b model). The typical curvature of the resulting stress-strain-curve arises from superposition of these terms. One term describes inter-crystalline creep along grain boundaries. Another one describes intra-crystalline dislocation reactions and the last one the behaviour at high temperatures ($T > 100$ °C) (Günther, et al., 2016).

For tertiary creep damage part $\dot{\varepsilon}_{cr}^d$ is assumed to correspond to the dilatancy rate $\dot{\varepsilon}_{vol}$. Dilatancy ε_{vol} is mainly influenced by minimum stress σ_3 and dilatancy work U_{dil} . To take tertiary creep into account in eq. 32 exponent η_p is described by a function $\eta_p(\sigma_3, \varepsilon_{vol})$. Elastic behaviour also depends on dilatancy, therefore elastic parameters E and ν or K and G resp., are functions of ε_{vol} in the G/S model. Furthermore, the model includes approaches to describe tensile failure and recovery (Salzer, 1993; Salzer, Konietzky & Günther, 1998; Günther, 2009).

- **Minkley model**

The Minkley model is a combination of the modified Burgers-model with a plastic model. The total visco-plastic distortion rate is therefore a result of the damage-free creep rate of the modified Burgers-model and the damage induced incremental plastic deformation. The resulting creep rate combines the terms of the Kelvin- and Maxwell-creep $\dot{\varepsilon}_{cr}^K = \dot{\varepsilon}_{cr}^p$ and $\dot{\varepsilon}_{cr}^M = \dot{\varepsilon}_{cr}^s$ and $\dot{\varepsilon}_{cr} = \dot{\varepsilon}_{cr}^s + \dot{\varepsilon}_{cr}^p$.

$$\dot{\varepsilon}_{cr}^p(t) = \frac{\sigma_{eff}}{3\eta_K} \cdot e^{\left(\frac{-G_K t}{\eta_K}\right)} \quad (44)$$

$$\dot{\varepsilon}_{cr}^s = \frac{\sigma_{eff}}{3\eta_{M,0}} \cdot e^{(-m \cdot \sigma_{eff})} \quad (45)$$

Recent investigations (Günther, et al., 2016) have shown, that especially with small difference stresses stationary creep rate is underestimated by the exponential approach given in eq. 45. That is why in recent publications Sinus-Hyperbolicus function is used instead (Minkley, Bérest, Schleinig, Farkas, & Böttge, 2012).

$$\dot{\varepsilon}_{cr}^s = \frac{\sigma_{eff}}{3\eta_{M,0}} \cdot \sinh(m \cdot \sigma_{eff}^n) \quad (46)$$

The behaviour at different temperatures is considered in the Maxwell viscosity with the well-known Arrhenius term where η_{M,T_0} is the viscosity-temperature-constant.

$$\eta_{M,0}(T) = \eta_{M,T_0} \cdot e^{\left(\frac{Q}{R \cdot T}\right)} \quad (47)$$

In eq. 44 to eq. 46 G_K is the Kelvin shear modulus, η_K/η_M are Kelvin / Maxwell viscosities and m , l and n are dimensionless parameters characterizing the stress dependency. In the model a plastic correction is included, where volume change is calculated by dilation function N_ψ and multiplier λ_s (Günther, et al., 2016).

$$\Delta \varepsilon_{vol}^{pl} = \lambda_s \cdot (1 - N_\psi) \quad (48)$$

Elastic parameters K and G_M are turned into functions of ε_{vol}^{pl} in the Minkley model to consider dilatancy dependence. Furthermore, the model includes approaches to describe tensile failure and recovery.

- **Döring/Kiehl model / TUBSSalt model**

The Döring/Kiehl model (Döring & Kiehl, 1996) is a rheological model including primary, secondary, tertiary creep and description of shear- and tensile failure as well as for post-failure behaviour (Wittke, 2014). The model was further developed to TUBSSalt model (Missal, Gährken, & Stahlmann, 2016).

$$\begin{aligned} \{\dot{\varepsilon}_{cr}^p\} &= \frac{1}{\eta_p^*} (\sigma_{eff} \cdot q_p)^{n_p} \cdot (\varepsilon_{eff}^{max} - \varepsilon_{eff}) \cdot \frac{\partial \sigma_{eff}}{\partial \{\sigma\}} \\ \{\dot{\varepsilon}_{cr}^s\} &= \frac{q_s}{\eta_s} \cdot \sigma_{eff}^{(n_s \cdot q_s^*)} \cdot \frac{\partial \sigma_{eff}}{\partial \{\sigma\}} \end{aligned} \quad (49)$$

In this model the viscosity for primary creep increases with increasing hardening. The temperature dependency is implemented in form of temperature coefficients q_x with reference temperature T_0 .

$$\begin{aligned} q_p &= \left(\frac{T}{T_0}\right)^2 \\ q_s^* &= \left(\frac{T}{T_0}\right)^{\frac{2}{3}} \\ q_s &= \left(\frac{T}{T_0}\right) \cdot \frac{e^{\left(\frac{-Q}{R \cdot T}\right)}}{e^{\left(\frac{-Q}{R \cdot T_0}\right)}} \end{aligned} \quad (50)$$

- **SUVIC model**

The SUVIC model (Strain rate history-dependent Unified Viscoplastic model with internal variables for Crystalline materials) is a unified model with internal state variables B , R and K (Aubertin, Gill, & Ladanyi, 1991).

$$\dot{\epsilon}_{cr} = A \cdot \left(\frac{\sigma - B + R}{K} \right)^n \quad (51)$$

Since its first version, several modifications have been performed. Like in the Minkley model stationary creep is described by Sinus-Hyperbolicus function in most recent versions of the SUVIC model (Boulianne, Simon, & Aubertin, 2004).

7 References

- Aubertin, M., Gill, D. E., & Ladanyi, B. (1991). An internal variable model for the creep of rocksalt. *Rock Mechanics and Rock Engineering*, 24, 81-97.
- Baar, C. A. (2013). *Applied salt-rock mechanics 1: the in-situ behavior of salt rocks* (Vol. 16). Elsevier.
- Backhaus, G. (1983). *Deformationsgesetze: mathematische und physikalische Grundlagen, elastisches und inelastisches Materialverhalten, große Verformungen, Fließvorgänge, Elastizität und Viskoelastizität, Plastizität und Viskoplastizität*. Akad.-Verlag.
- Blum, W. (1978). *Gleitung und Erholung während plastischer Verformung kristalliner Stoffe bei hoher Temperatur*. Habilitationsschrift, Universität Erlangen-Nürnberg.
- Boresi, A. P., & Deere, D. U. (1963). Creep closure of a spherical cavity in an infinite medium. *final report to Holmes and Narver, Inc., Las Vegas Division*.
- Boulianne, M., Simon, R., & Aubertin, M. (2004). A numerical investigation of the creep (viscoplastic) behaviour of circular opening and pillar in rock salt. *57th Canadian geotechnical conference and the 5th joint CGS-IAH conference*.
- D'Ans, J., & Lax, E. (1967). *Taschenbuch für Chemiker und Physiker: Makroskopische physikalisch-chemische Eigenschaften*. (E. Lax, Ed.) Springer.
- Döring, T., & Kiehl, J. R. (1996). Das primäre, sekundäre und tertiäre Kriechen von Steinsalz - Ein dreidimensionales rheologisches Stoffgesetz. *Geotechnik*, 3, 194-199.
- Elliger, C. (2005). *Untersuchungen zum Permeationsverhalten von Salzlaugen in Steinsalz bei der Endlagerung wärmeentwickelnder nuklearer Abfälle*. Ph.D. dissertation, Technische Universität Darmstadt.
- Fokker, P. A. (1998). The micro-mechanics of creep in rocksalt. *The Mechanical Behavior of Salt, Proceedings of the 4th Conference, Montreal, 1996* (pp. 49-61). Trans Tech Publications, Clausthal-Zellerfeld.
- Fossen, H. (2016). *Structural geology*. Cambridge University Press.
- Günther, R. M., Lüdeling, C., Popp, T., Naumann, D., Wiedemann, M., & Weise, D. (2016). Vergleich aktueller Stoffgesetze und Vorgehensweisen anhand von Modellberechnungen zum thermo-mechanischen Verhalten und zur Verheilung von Steinsalz. *BMBF-Verbundvorhaben, Einzelbericht zum Teilvorhaben 2*.
- Günther, R.-M. (2009). *Erweiterter Dehnungs-Verfestigungs-Ansatz: phänomenologisches Stoffmodell für duktile Salzgesteine zur Beschreibung primären, sekundären und tertiären Kriechens*. Ph.D. dissertation, Institut für Geotechnik, Technische Universität Bergakademie Freiberg.
- Hahn, F. (2003). *Untersuchung des zyklisch plastischen Werkstoffverhaltens unter umformnahen Bedingungen*. Ph.D. dissertation, Fakultät für Maschinenbau, Technische Universität Chemnitz.
- Hampel, A., Heemann, U., Schulze, O., Zetsche, F., Pudewills, A., Günther, R., . . . others. (2007). Die Modellierung des mechanischen Verhaltens von Steinsalz: Vergleich aktueller Stoffgesetze und Vorgehensweisen. *BMBF-Verbundvorhaben, Synthesebericht, Förderkennzeichen 02 C 1004 bis 2 C 1054*.

- Hou, Z. (1997). *Untersuchungen zum Nachweis der Standsicherheit für Untertagedeponien im Salzgebirge*. Technische Universität Clausthal, Professur für Deponietechnik und Geomechanik. Papierflieger.
- Hunsche, U. (1996). *Thermomechanisches Verhalten von Salzgesteinen*. Tech. rep., Abschlussbericht zum Forschungsvorhaben der BGR für das BMBF, Hannover .
- Hunsche, U., & Hampel, A. (1999). Rock salt--the mechanical properties of the host rock material for a radioactive waste repository. *Engineering geology*, 52, 271-291.
- Hunsche, U., & Schulze, O. (1994). Das Kriechverhalten von Steinsalz. *Kali und Steinsalz*, 11, 238-255.
- Hunsche, U., & Schulze, O. (2003). The dilatancy concept--a basis for the modelling of coupled TMH processes in rock salt. *European Commission CLUSTER Conference on the Impact of EDZ on the Performance of Radioactive Waste Geological Repositories, Luxembourg*, (pp. 102-109).
- Lux, K.-H. (1984). *Gebirgsmechanischer Entwurf und Felderfahrungen im Salzkavernenbau: ein Beitrag zur Entwicklung von Prognosemodellen für den Hohlraumbau im duktilen Salzgebirge*. F. Enke Verlag.
- Menzel, W., & Schreiner, W. (1975 - 1978). Zum geomechanischen Verhalten von Steinsalz verschiedener Lagerstätten der DDR. *Neue Bergbautechnik*, 8, 143-148.
- Menzel, W., & Schreiner, W. (1977). Zum geomechanischen Verhalten von Steinsalz verschiedener Lagerstätten der DDR. Teil II: Das Verformungsverhalten. *Neue Bergbautechnik*, 7, 565-571.
- Minkley, W., Bérest, P., Schleinig, J. P., Farkas, F., & Böttge, V. (2012). Dynamic back-calculation of the collapse of the Saint-Maximilien mining field during mining on rock salt in Varangéville (1873). *Mechanical Behaviour of Salt VII*, 241.
- Missal, C., Gährken, A., & Stahlmann, J. (2016). Vergleich aktueller Stoffgesetze und Vorgehensweisen anhand von Modellberechnungen zum thermo-mechanischen Verhalten und zur Verheilung von Steinsalz. *BMBF-Verbundvorhaben, Einzelbericht zum Teilvorhaben 6*.
- Munson, D. E., & Dawson, P. R. (1979). *Constitutive model for the low temperature creep of salt (with application to WIPP)*. Tech. rep., Sandia Labs., Albuquerque, NM (USA).
- Munson, D. E., & Dawson, P. R. (1984). Salt-constitutive modeling using mechanism maps. *The Mechanical Behavior of Salt, Proceedings of the 1st Conference, Pennsylvania State University, 1981* (pp. 717-737). Trans Tech Publications, Clausthal-Zellerfeld.
- Norton, F. H. (1929). *The creep of steel at high temperatures*. McGraw-Hill Book Company.
- Odé, H. (1968). Review of Mechanical Properties of Salt Relating to Salt-Dome Genesis. *Saline Deposits -- Geol. Soc. Am. Spec. Pap.*, (pp. 543-595).
- Odqvist, F. K., & Hult, J. (1962). *Kriechfestigkeit metallischer Werkstoffe*. Springer-Verlag.
- Paturi, F. R., F. S., & Herholz, M. (1991). *Die Chronik der Erde*. Weltbild Verlag.

- Popp, T. (2002). Transporteigenschaften von Steinsalz--Modellierung der Permeabilitäts-Porositäts-Beziehung. *Meyniana*, 54, 113-129.
- Salzer, K. (1993). *Ableitung eines kombinierten Kriechgesetzes unter Berücksichtigung der Erholung*. Tech. rep., IfG Leipzig.
- Salzer, K., Konietzky, H., & Günther, R.-M. (1998). A new creep law to describe the transient and secondary creep phase. In *Application of Numerical Methods to Geotechnical Problems* (pp. 377-387). Springer.
- Schoenherr, J., Schléder, Z., Urai, J. L., Fokker, P. A., & Schulze, O. (2007). Deformation mechanisms and rheology of Pre-cambrian rocksalt from the South Oman Salt Basin. *The Mechanical Behaviour of Salt -- understanding of THMC processes in salt, Hannover, 2007* (pp. 167-173). Taylor & Francis, London.
- Wagner, G. (1999). *Plastische Verformung von LiF-Einkristallen, polykristallinem Kupfer und Stahl*. Zulassungsarbeit zum ersten Staatsexamen für das Lehramt an Gymnasien im Bereich Physik, Lehrstuhl für Experimentalphysik I, Universität Augsburg.
- Wang, G. (2004). A new constitutive creep-damage model for salt rock and its characteristics. *International Journal of Rock Mechanics and Mining Sciences*, 41, 61-67.
- Wawersik, W. R. (1988). Alternatives to a power-law creep model for rock salt at temperatures below 160°C. *The Mechanical Behavior of Salt, Proceedings of the 2nd Conference, Hannover, 1984* (pp. 103-128). Trans Tech Publications, Clausthal-Zellerfeld.
- Wittke, W. (2014). *Rock mechanics based on an anisotropic jointed rock model (AJRM)*. John Wiley & Sons.
- Wright, J., & Colling, A. (1995). *Seawater: Its Composition, Properties and Behaviour* (2nd ed.). Elsevier.